A 2.67 µJ per Measurement FMCW Ultrasound Rangefinder System for the Exploration of Enclosed Environments

A 2.67 μJ per Measurement FMCW Ultrasound Rangefinder System for the Exploration of Enclosed Environments

Gönenç Berkol, *Student Member, IEEE*, Peter G. M. Baltus, *Senior Member, IEEE*, Pieter J. A. Harpe, *Senior Member, IEEE*, and Eugenio Cantatore, *Fellow, IEEE*

***Abstract*—This letter presents the design and experimental characterization of an ultrasound rangefinder system. A new distance measurement method is proposed for determining the relative position among sensor nodes that are operated in a collision and multipath rich environment, while needing no common time reference between them. A 65 nm CMOS technology has been used to build the sensor nodes, which comprise an on-chip receiver and transmitter. The proposed rangefinder system is characterized up to 1 m in air and has a range resolution of 6.5 mm, while dissipating 2.67 μJ per measurement.**

***Index Terms*—Analog IC, swarm of sensor nodes, ultrasound (US) rangefinder, ultrasound front-end, ultrasound receiver.**

I. Introduction

Exploration of environments that are inaccessible and miss GPS coverage is an emerging application, where the information on the geometry of enclosed volumes, such as underground reservoirs, or water and oil pipelines, is desired. Swarms of sensor nodes can be used for this exploration. The nodes are injected into the volume to explore, where they perform distance measurements while traversing the unknown environment with the flow of the medium [1]. Afterward, the nodes are recuperated and the data in their memories are analyzed, to build a map of the environment visited based on the distances measured between the nodes during the exploration [2]. Ultrasound (US) has been used as a way to exchange data in fluidic environments due to its favorable propagation characteristic in liquids compared to RF. Typical approaches to US distance measurement are based on the time of flight (ToF) of the reflected echoes. In the described application, however, it is desired to measure the distances between nodes, while echoes from passive reflectors in the environment should be neglected. This problem is addressed in this letter by devising a novel rangefinder system based on a US frequency-modulated continuous-wave (FMCW) method to determine the distance between nodes in a swarm. Moreover, the measurement method described does not require global clock synchronization within the swarm. This letter is organized as follows. Section II explains the details of the proposed rangefinder system. In Sections III and IV, the system and circuit design are discussed. The measurement results are presented in Section V. The performance of the US transceiver is benchmarked against prior art and conclusions are given in Section VI.

Manuscript received May 18, 2020; revised July 9, 2020 and July 30, 2020; accepted August 19, 2020. Date of publication August 24, 2020; date of current version September 11, 2020. This article was approved by Associate Editor Piet Wambacq. This work was supported by the European Unions Horizon 2020 Research and Innovation Programme under Grant 665347. *(Corresponding author: Gönenç Berkol.)*

The authors are with the Electrical Engineering Department, IC Group, Eindhoven University of Technology, 5600 MB Eindhoven, The Netherlands (e-mail: g.berkol@tue.nl).

Digital Object Identifier 10.1109/LSSC.2020.3018791

II. Proposed Rangefinder System

Each sensor node has an on-chip RX and TX for receiving and broadcasting US data, as shown in Fig. 1(a). An FPGA is used here as a digital backend, which initiates the ranging operation and controls the operating mode of the sensors. The nodes use two off-chip transducers, T1 and T2, which can be connected to either the TX or RX using an off-chip switching matrix. The nodes enable two different modes of operation. The default mode is called the active tag mode. The nodes operating as an active tag listen to the incoming signals via the transducer T1, and actively transmit back a modified version of the incoming signal by using the transducer T2. The second operating mode is called the ranger mode, where a node aims to find the distance of the surrounding active tags. The digital backend of a sensor node activates the ranger mode periodically, to initiate the distance measurement protocol. The initiation does not need a global synchronization among nodes in the system and can be activated anytime based on an algorithm inside the digital backend. The distance measurement is performed by means of a two-way ranging using frequency-modulated US signals. The conventional FMCW ranging method is shown in Fig. 2(a). A chirp, a signal with a linearly changing frequency in time, is transmitted, and its reflected echo is received after a time τ_d. The spectrum of the signal obtained mixing the sent and received chirps will show a frequency peak, f_{beat}, corresponding to the round trip time, τ_d, of the echo chirp. As we would like to find the distance to the active tags and avoid the echoes from the boundary of the environment, a modified version of the conventional method is proposed, as shown in Fig. 2(b). Its principle can be explained as follows. The ranger node generates two chirp signals, Chirp1r and Chirp2r. Chirp1r fits the bandwidth (BW) of T1, and Chirp2r fits the BW of T2, which do not overlap. Chirp1r is broadcasted via T1, and reaches the other nodes that are operating as active tags. These nodes downmodulate the Chirp1r to baseband and upmodulate it again to a frequency band fitting T2, named as the Chirp2t. This signal is sent back using T2 and reaches the ranger node, where it is multiplied by the original Chirp2r. The resulting spectrum, similar to the conventional method, will have a frequency beat corresponding to the round trip delay between the nodes. As a result, with knowledge of the BW and the duration (T_{sweep}) of the chirps, as well as the speed of US in the medium, the distance to the active tags is calculated (Fig. 2). Thanks to the different frequencies of the signal sent by the ranger and the signal sent back by the active tag, the ranger node can distinguish echoes coming from passive reflectors from signals sent back by active tags. In case multiple active tags are present at different distances, different frequency peaks corresponding to the active tags will be obtained [3]. By adding a different identification payload to the chirp in each active tag, the ranger can also distinguish between the first signal received by a tag and possible later signals coming from the same tag due to multipath.

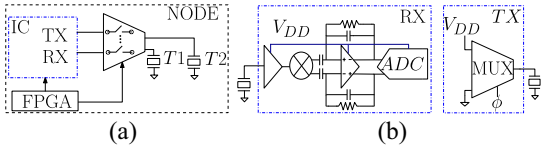

Fig. 1. (a) Building blocks of a sensor node. (b) Top-level implementation of the corresponding blocks.

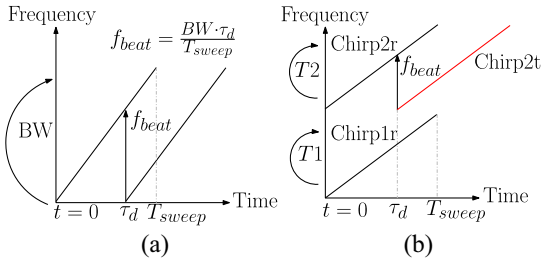

Fig. 2. (a) Conventional FMCW method. (b) Proposed method.

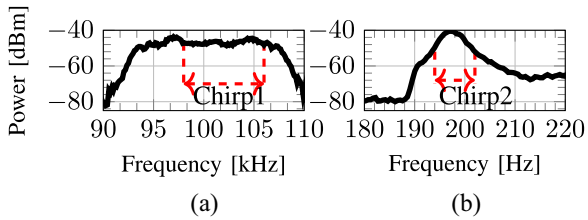

Fig. 3. Link characterization of (a) T1 and (b) T2. Each measurement is performed at 10-cm distance.

III. System Design

The intended operating medium for the rangefinder system is fluidic, where US propagates with much lower attenuation (<100×) compared to air. However, to simplify measurements and keep the maximum distance between the sensor nodes at a manageable level, we built the proof-of-concept characterization setup of the proposed system in air. Accordingly, considering that the duration of the chirp has to be larger than the round trip (≈ 6 ms) among the sensors at the desired maximum distance, which is chosen as 1 m in air, T_{sweep} is determined as 8 ms. With this choice, a maximum distance of 6 m can be achieved in water. If c_{US} is the speed of sound in air and BW is the bandwidth of the chirp signals, the smallest distance step that can be measured using FMCW is ($c_{US}/2BW$). To keep it about 20 mm, a chirp BW of 8 kHz is needed in air. T1 and T2 are commercially available piezoelectric transducers [4] chosen to broadcast and receive the above-mentioned chirps. T1 and T2 have a size of $40\times40\times17$ mm and $19\times19\times11$ mm, a parasitic capacitance of 0.88 and 1.1 nF, and a nominal resonance of 100 and 200 kHz, respectively. The link among the transducers is characterized by exciting them with a 0.6 V_{pp} square-wave signal and recording the electrical power received with identical transducer, as shown in Fig. 3. Due to the narrowband characteristic of T2, the frequency range between 194 and 202 kHz corresponding to its 10-dB BW has been assigned for Chirp2, while Chirp1 occupies the range between 98 and 106 kHz residing inside the 6-dB BW of T1. The link-budget analysis has been performed by investigating the power loss of the transducers in air at room temperature, where T1 and T2 are driven with a 0.6 V_{pp} burst signal at their resonance. The received power is modeled with the formula: $P_{\text{rec}} = -k \cdot 10\log(d) + P_0$, where d is the distance in cm, k is the path-loss coefficient, and P_0 is the initial power loss (Table I).

TABLE I
System Specifications

Parameter	Value
$f_{Resonance}$	100kHz (T1), 200kHz (T2)
Distance in air	1m
T_{sweep}	8msec
V_{DD}	0.6V
BW	8kHz
$P_{rec,T1}$	$-1.7 \cdot 10log(d) - 30.37$ (dBm)
$P_{rec,T2}$	$-2.2 \cdot 10log(d) - 20.1$ (dBm)
SNR_{in}	>12dB
IRN_{RX}	<9μV_{rms}
f_{beat}	<6kHz

Accordingly, the power received for a link built with two T2 transducers at 1 m distance in air is measured as −64 dBm. Considering that T2 will be used within its 10-dB BW and reminding that ≈12 dB SNR at the input of the receivers is needed to have a 90% detection probability with a $<10^{-3}$ false alarm ratio [5], the required RX integrated noise should be lower than 9 μV_{rms}. As reported in Table I, using the above-mentioned system settings, an f_{beat} of ≈6 kHz is estimated at 1 m, which has to reside inside the BW of the RX. The link losses for T1 at 1 m are very similar, but the attenuation provided by that transducer is lower, and thus the RX noise level is defined by the link using T2.

IV. Circuit Design

Fig. 1(b) shows the top-level implementation of the RX, which comprises a single-ended inverter-based low-noise amplifier (LNA), a single-balanced passive mixer (SBPM), a closed-loop baseband amplifier (BBAMP), and a 10-bit SAR ADC, all sharing a single supply, V_{DD}, of 0.6 V. The output of the LNA is dc coupled to the SBPM, which uses two nMOS transistors as a switch. After the high-frequency harmonics of the mixer are filtered by the BBAMP, the signal is converted to the digital domain by a 10-bit SAR ADC, which has been presented in detail in [6]. The nonlinearity and noise level of the ADC are negligible for overall RX performance. A single-ended, open-loop topology is chosen in the LNA to save power and reduce the effect on the input noise of the rest of the front-end. Stabilizing the output dc voltage of the inverter-based amplifiers requires a dc feedback [7], [8]. In this design, as shown in Fig. 4(a), the dc feedback is applied using an error amplifier (EA) and an auxiliary inverter, formed by M_{p1} and M_{p2}, put in parallel to the main input inverter (M_1, M_2). The auxiliary inverter is current starved with the transistors M_{cs1} and M_{cs2} to limit its power consumption. M_1 and M_2 are ac coupled to the transducers input, RX_{in}, and these transistors are separately biased. The dc gate voltages of M_1, M_{cs1}, M_2, and M_{cs2} are provided via pseudoresistors and internal current mirrors. The EA is designed as a differential pair with active load and uses the same supply of V_{DD} as in the LNA. To save power and to increase the output impedance, the transconductance of the auxiliary inverter is made much lower than the one of M_1 and M_2. All transistors in the LNA, bias network, and the EA are biased in the weak-inversion region to maximize their g_m/I_D ratio. The proposed dc feedback method can compensate the errors due to mismatch in the biasing network and the LNA. Simulations predict that the output voltage is stabilized to V_{ref} with less than a 10 mV error across PVT, when an ideal $V_{\text{ref}} = (V_{DD}/2)$ is used. The BBAMP uses a two-stage architecture with Miller compensation and provides a gain of 12 dB determined by a capacitive feedback network [Fig. 1(b)]. The complete front-end is simulated to have a conversion gain of 43 dB, a BW of 20 kHz, and an IRN of 7.8 μV_{rms} while using a single 0.6 V supply. The TX is designed as a simple multiplexer and comprises two nMOS transistors that connect the desired dc voltage to the transducer load, as

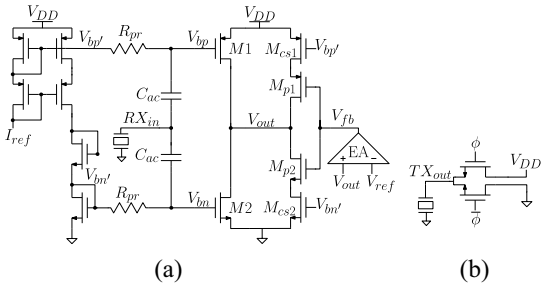

Fig. 4. Schematic of the (a) LNA and its biasing network. (b) Output multiplexer as a TX.

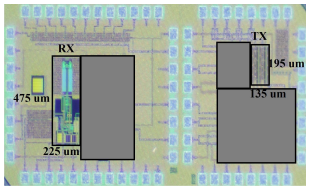

Fig. 5. Die photograph of the RX and the TX. Only chip areas that are relevant to this letter are shown.

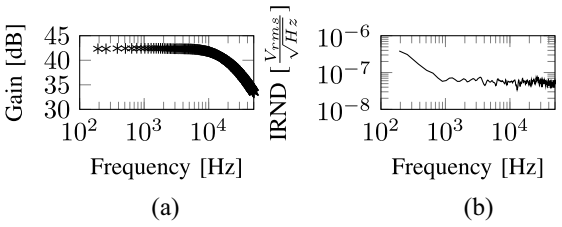

Fig. 6. (a) Measured conversion gain of the RX. The maximum gain is 42.4 dB @1 kHz and the 3-dB BW is 21.4 kHz. (b) Input-referred noise density (IRND) of the RX. IRND = 60 $nV_{\text{rms}}/\sqrt{Hz}$@1 kHz is measured.

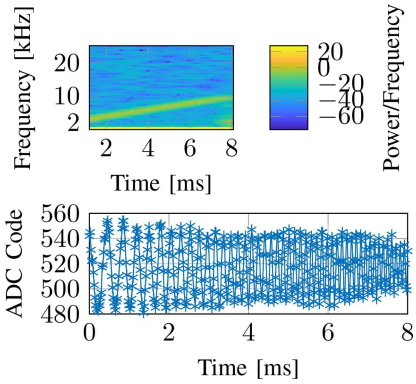

Fig. 7. Top: Spectrogram of the downconverted chirp of the active tag. Bottom: The corresponding transient ADC output, coherent with the frequency-dependent attenuation of T1.

shown in Fig. 4(b). The switches are designed to avoid voltage division with the impedance of the transducers at their resonance. The period of the driving signal is controlled by activating the nonoverlapping clocks ϕ and $\overline{\phi}$, which are distributed to the switch transistors with on-chip buffers having a 1.2 V supply.

V. Measurement Results

A 65 nm CMOS process is used for fabrication and the die photographs of the RX and TX are shown in Fig. 5. The measured conversion gain and IRND of the RX are shown in Fig. 6(a) and

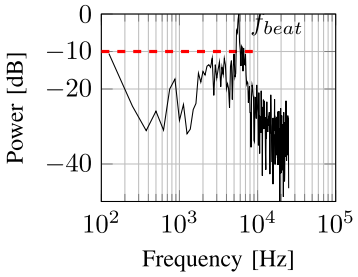

Fig. 8. Normalized spectrum of the measured ADC data at 1 m.

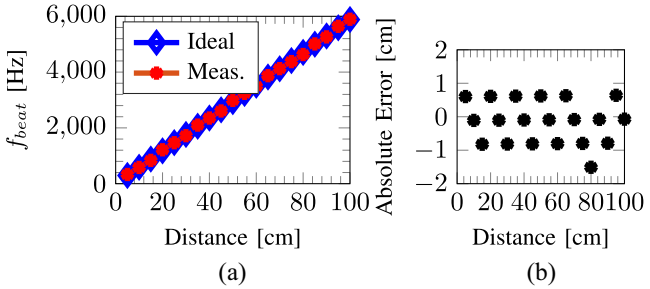

Fig. 9. (a) FMCW ranging link characterization. (b) Absolute error in the distance measurement.

(b), respectively. The RX has an IRN of 8.8 μV_{rms} in the band 125 Hz–21.4 kHz, which is sufficient for detecting beat frequencies at the target ranges. During characterization, an external reference current, I_{ref}, of 1 nA is used. The LO required for the active tag (96 kHz/192 kHz), the chirps for the ranger node, and the sampling clock (50 kHz) for the ADCs are provided by the FPGA, derived from an external oscillator. The integrated RX draws a total measured current of 930 nA from a 0.6 V supply, therefore, dissipates a total power of 0.56 μW. The TX dissipates 1.59 μJ per chirp when driving T2, and dissipates 1.07 μJ per chirp when it drives T1. The measured TX efficiency (power transferred to the transducer as a fraction of the power required from the supply) when driving T1 and T2 with the chirp signals is 58% and 44%, respectively. The proposed rangefinder system requires 2.67 μJ energy per distance measurement. This figure includes the power of the on-chip buffers used to distribute and drive the chirps, the control phases of the TX, and the sampling clock of the ADC. It excludes the digital power, the losses in the power management, and the power needed for the generation of the on-chip current references and clocks. The baseband output of the active tag RX is recorded when the tag receives Chirp1r via T1. The corresponding transient output of the ADC and its spectrogram are shown in Fig. 7, where the broadcasted chirp BW of 8 kHz can be appreciated. The active tag then upmodulates this chirp by simply XORing the ADC code with the fixed frequency $2 \cdot \text{LO} = 192$ kHz, and broadcasts the resulting signal via T2. The spectrum of the data recorded by the ranger node after mixing the received Chirp2t with the original Chirp2r at 1 m distance in air is depicted in Fig. 8, where the highest frequency peak is defined as f_{beat}. To reduce the complexity in the digital domain, no additional filters are used, and the mixing spurs of the image chirp are also visible in the spectrum. A proof-of-concept characterization of the proposed rangefinder system up to 1 m in air is summarized in Fig. 9(a), and the calculated absolute distance error is depicted in Fig. 9(b). The standard deviation of the absolute error is found to be 6.5 mm. The FFT resolution is equal to the inverse of the T_{sweep}, which is 125 Hz. This provides a minimum measurable distance (d_{min}) of 21 mm and a theoretical measurement resolution (standard deviation of the error

TABLE II
PERFORMANCE COMPARISON OF THE PROPOSED US RANGEFINDER

	[10]	[9]	**This Work**	
Method	ToF	Phase-shift	FMCW	
Target Reflector	Passive	Passive	Active	
Transducers	PMUT	Membrane	PZT	
Technology [nm]	180	800	65	
Min/Max Range [mm/m]	45/1	18/0.11	50/1	
Range Error [mm]	0.41 @0.5m	2.5@0.1m	6.5@1m	
Field of view	3D	1D	1D	
TX Supply [V]	32	5	0.6 + 1.2	
			T1	T2
Frequency [kHz]	220	100	98-106	194-202
TX Energy Consumption [μJ]	1.05	2800	1.07	1.59
RX Supply [V]	1.8	5	0.6	0.6
RX Energy Consumption [μJ]	1.6	3700	0.004	0.004
Total Energy per Measurement [μJ]	2.65[a]	6500	2.67	

a: Energy consumption is scaled per channel excluding the power overhead of the digital circuits.

distribution) of $(d_{\min}/\sqrt{12}) = 6.1$ mm, which is in good agreement with the value determined experimentally. The memory needed for one measurement is 4 kb.

VI. BENCHMARK AND CONCLUSION

The performance of the proposed US rangefinder and its comparison with the prior art is summarized in Table II. The work in [9] is based on the detection of phase shift, and the work in [10] is based on a ToF measurement of the echoes coming from passive reflectors in air. Contrary to the prior art, this work enables the US distance measurement between active tags while minimizing interference from passive reflectors. For this purpose, our work uses two separate frequency bands to distinguish the active responses from the passive reflections of the environment. In our work, due to the narrowband transducers used to broadcast the chirps, the range resolution of the distance measurement is 6.5 mm, which is tolerable in the applications considered. Thanks to the power-aware design methodology for the rangefinder system described in this letter, our work dissipates 2.67 μJ per measurement. The response of the active tags will be transmitted only when they receive a signal in a separate frequency band, thus their operation is independent of each other and the need of a global synchronization is eliminated. The extraction of distance information from raw ADC data is done outside the nodes, after recuperating them. The energy needed to write the raw data in a memory and the power needed to keep them can be negligible when compared, respectively, to the measurement energy and the normally on node power [11].

REFERENCES

[1] E. H. A. Duisterwinkel, G. Dubbelman, E. Talnishnikh, J. J. W. M. Bergmans, H. J. Wörtche, and J. M. G. Linnartz, "Go-with-the-flow swarm sensing in inaccessible viscous media," *IEEE Sensors J.*, vol. 20, no. 8, pp. 4442–4452, Apr. 2020.

[2] S. Schlupkothen, A. Hallawa, and G. Ascheid, "Evolutionary algorithm optimized centralized offline localization and mapping," in *Proc. IEEE Int. Conf. Comput. Netw. Commun. (ICNC)*, Maui, HI, USA, 2018, pp. 625–631.

[3] S. Roehr, P. Gulden, and M. Vossiek, "Precise distance and velocity measurement for real time locating in multipath environments using a frequency-modulated continuous-wave secondary radar approach," *IEEE Trans. Microw. Theory Techn.*, vol. 56, no. 10, pp. 2329–2339, Oct. 2008.

[4] (2020). *MCUSD40A100B17RS70C-MCUSD19A200B11RS Multicomp Ultrasonic Sensors*. [Online]. Available: https://uk.farnell.com /multicomp-ultrasonic-transducers

[5] M. I. Skolnik, *RADAR Systems*. New York, NY, USA: McGraw-Hill, 2001.

[6] P. J. A. Harpe, H. Gao, R. van Dommele, E. Cantatore, and A. H. M. van Roermund "A 0.20 mm^2 3 nW signal acquisition IC for miniature sensor nodes in 65 nm CMOS," *IEEE J. Solid-State Circuits*, vol. 51, no. 1, pp. 240–248, Jan. 2016.

[7] C. Chen, Z. Chen, Z. Chang, and M. A. P. Pertijs, "A compact 0.135-mW/channel LNA array for piezoelectric ultrasound transducers," in *Proc. 41st Eur. Solid-State Circuits Conf. (ESSCIRC)*, Graz, Austria, 2015, pp. 404–407.

[8] G. Berkol, P. G. M. Baltus, P. J. A. Harpe, and E. Cantatore, "A -81.6dBm sensitivity ultrasound transceiver in 65nm CMOS for symmetrical data-links," in *Proc. IEEE 45th Eur. Solid State Circuits Conf. (ESSCIRC)*, Cracow, Poland, 2019, pp. 145–148.

[9] C. Kuratli and Q. Huang, "A CMOS ultrasound range-finder microsystem," *IEEE J. Solid-State Circuits*, vol. 35, no. 12, pp. 2005–2017, Dec. 2000.

[10] R. J. Przybyla, H.-Y. Tang, A. Guedes, S. E. Shelton, D. A. Horsley, and B. E. Boser, "3D ultrasonic rangefinder on a chip," *IEEE J. Solid-State Circuits*, vol. 50, no. 1, pp. 320–334, Jan. 2015.

[11] Q. Dong *et al.*, "11.2 a 1Mb embedded NOR flash memory with 39μW program power for mm-scale high-temperature sensor nodes," in *Proc. IEEE Int. Solid-State Circuits Conf. (ISSCC)*, San Francisco, CA, USA, 2017, pp. 198–199.